An Investigation into the Spatial Variability of Near-Surface Air Temperatures in the Detroit, Michigan, Metropolitan Region*

EVAN M. OSWALD AND RICHARD B. ROOD

Department of Atmospheric, Oceanic and Space Sciences, University of Michigan, Ann Arbor, Michigan

KAI ZHANG, CARINA J. GRONLUND, MARIE S. O'NEILL, AND JALONNE L. WHITE-NEWSOME

School of Public Health, University of Michigan, Ann Arbor, Michigan

SHANNON J. BRINES AND DANIEL G. BROWN

School of Natural Resources and Environment, University of Michigan, Ann Arbor, Michigan

(Manuscript received 23 June 2011, in final form 28 November 2011)

ABSTRACT

On an annual basis, heat is the chief cause of weather-related deaths in the United States. Therefore, understanding the temperature structure where people live is important for reducing the health burden imposed by hot weather. This study focused on the air temperatures in the Detroit, Michigan, metropolitan region during the summer of 2009. An observational network was established that included 1) monitors sited in the backyards of residential participants, 2) National Weather Service standard observations, and 3) a network of monitors operated by the State of Michigan. Daily high and low temperatures were analyzed for spatial pattern, magnitude of spatial variability, and relationships with weather conditions. The existence of spatial variability was confirmed specifically during weather that was considered to be dangerous to public health. The relationships between temperature observations and distance to water, distance to city center, and local percent of impervious surface were investigated. The spatial variability during the daily low was typically stronger in magnitude and the spatial pattern was more consistent than were those during the daily high. The largest correlation with land-cover and location attributes was between values of percent of impervious surface and daily low temperatures. Daily high temperatures were most correlated with distance to water. Consistent with previous studies on spatial variability in urban environments, the results suggest a need for sensitivity to the spatially variable nature of exposure to heat events in both public health and urban planning. For example, these results showed that the downtown area experienced elevated temperatures during nights and that the eastern portions of Detroit experienced decreased temperatures during afternoons.

1. Introduction

In 2010, more than one-half of the world's population was estimated to live in urban regions, with a projection of 70% by 2050 (United Nations Population Division 2010). Heat is a leading annual cause of natural weather-related fatalities (NWS Office of Climate, Weather, and Water Services 2010b), and city size has been correlated with the magnitude of temperature alteration by cities (Oke 1973; Stone et al. 2010). Therefore, the importance of studying urban climates and health-related urban climate factors is increasing in both the fields of public health and atmospheric science.

Standard observational and forecast products of the National Weather Service (NWS) typically trigger watches and warnings about dangerously hot weather (NWS Office of Climate, Weather, and Water Services 2010a) in metropolitan regions. The meteorological monitors are often located at the official recording sites of the NWS and are specifically sited to avoid the effects of developed land cover (Observing Systems Branch 1989; Peterson 2003). Developed land cover

* Supplemental information related to this paper is available at the Journals Online website.

Corresponding author address: Evan Oswald, Dept. of Atmospheric, Oceanic and Space Sciences, University of Michigan, 2455 Hayward St., Ann Arbor, MI 48109-2143.
E-mail: eoswald@umich.edu

DOI: 10.1175/JAMC-D-11-0127.1

can alter the air temperatures and cause the urban heat island (UHI) effect, defined as the elevated temperatures within urban environments relative to the surrounding rural areas (Oke 1982). The UHI effect is well understood (Oke 1982; Bonan 2008; Grimmond et al. 2010). In general, studies focusing on either the UHI effect or spatial variability of air temperatures use either a pair (Ackerman 1985; Magee et al. 1999) or several fixed stations (Gedzelman et al. 2003; Basara et al. 2008) or use various forms of in situ transects (Wong and Yu 2005; Yokobori and Ohta 2009). Both spatial variability (at the local scale) and the UHI effect (at the mesoscale) are caused by differences between various land-cover types in heating rates and storage, latent and sensible heat flux partitioning, effectiveness of radiative energy exchanges and turbulent heat transport, and differences in downwelling radiative energy from gases and aerosols (Oke 1982).

Therefore, in addition to the urban–rural difference in temperature, significant spatial variability of air temperature also exists within developed regions (Bonan 2008). It has been suggested (Kunkel et al. 1996) that not enough studies investigate the variability of temperatures throughout a city during heat events. A recent study during a heat event in 2008 confirmed the existence of temperature spatial variability in Oklahoma City, Oklahoma (Basara et al. 2010). Knowledge of the sources and magnitude of variability is potentially useful to public-health practitioners and city planners to better identify parts of the city that are especially vulnerable to heat-related health threats (Wilhelmi et al. 2004).

One difficulty in taking urban ground-level meteorological observations is that the environmental surroundings can compromise the measurements. Networks of meteorological observing stations do exist within the urban and suburban environments and are typically run by utilities, educational institutions, transportation departments, and environmental quality agencies. Examples of such network data providers can be found at The University of Utah's MesoWest Database (e.g., http://mesowest.utah.edu/cgi-bin/database/stn_owner.cgi?owner=7 from the Utah Department of Transportation, http://mesowest.utah.edu/cgi-bin/database/stn_owner.cgi?owner=250 from the Oregon Department of Environmental Quality, and http://mesowest.utah.edu/cgi-bin/database/stn_owner.cgi?owner=345 from the WeatherForYou Internet site). The monitoring standards employed are unique to the specific purpose of each network. In addition, networks associated with private weather information providers such as Weather Underground and WeatherBug are designed to meet the requirements of the sponsoring organizations but frequently do not meet the more-rigorous observing standards (networkwide standardization, maintenance of calibration, and monitors not at rooftop level; Davey et al. 2002; Oke 2004) required to quantify the spatial variability of temperature. Although problems do exist, such nontraditional networks provide a potential resource to better characterize the highly variable structure of temperature that is found between the limited numbers of stations of standard meteorological observations within developed regions.

This study focuses only on the daily extremes of air temperature observed by a fixed network of several observing stations. The spatial variability of conventional air temperature, rather than a more sophisticated measure of physiological equivalent temperature (Steadman 1984; Jendritzky et al. 2001), is characterized because the results are more clear-cut. Neither the UHI effect nor spatial variability in temperature is typically largest during either daily high or low temperatures (Oke 1982); the spatial variability in the temperature is likely most important to public health during these daily extremes, however. The literature shows the daily high to be associated with both heat-related medical dispatches (Dolney and Sheridan 2006; Golden et al. 2008) and mortality rates (Basu 2009; Gosling et al. 2009). Daily minima are also associated with mortality rates, as are daily mean (often derived from the daily maximum and minimum) temperatures (Basu 2009; Gosling et al. 2009), although is not clear which of the three variables is more important. This has led to definitions of heat events that are based on these daily temperature extremes (Karl et al. 1996; Huth et al. 2000; Easterling et al. 2007). In addition, studies focusing on both heat events (Gershunov et al. 2009; Dole et al. 2011) and the UHI effect (Wilby 2003) have shown that they often occur during similar conditions (e.g., high pressure weather systems). The built environment affects both the daytime and overnight temperatures (Oke 1982; Grimmond and Oke 1995; Magee et al. 1999; Grimmond et al. 2010); therefore, understanding the spatial variations in both daily temperature extremes is important.

This study is part of a comprehensive study of heat and human health in Detroit, Michigan (Zhang et al. 2011). This study's first objective was to quantify and characterize the spatial variability in temperatures across the Detroit metropolitan region. Then, confirmation was sought of that spatial variability, specifically during hot weather. In addition, the relationships between three land-cover and location variables and the mean daily temperature extreme observations were investigated. It is hypothesized that relevant land-cover and location attributes may assist in the localization required to predict the spatial variability in temperature. The next

section describes the study area and the metrics for comparing observation data from different sources, followed by the methods.

2. Methods

a. Study area and climatological description

Detroit (42.33°N, 83.05°W), like all of southeastern Michigan, has a humid continental climate. The climate is affected by the city's proximity to the Great Lakes and its position on a major storm track; storms pass to the north during the summer, creating periods of warm, humid weather with sporadic thunderstorms that are followed by days of mild, dry weather. The land is effectively flat, rising lightly northwestward from the waterways, which are roughly 580 ft (177 m) above mean sea level. The 1980–2010 average number of cooling degree-days in Detroit was 167 in June, 271 in July, 225 in August, and 84 in September (National Weather Service 2011). Nearly 40 years have passed since the last published article that focused on the Detroit metropolitan region's UHI effect (Sanderson et al. 1973). Since then the city population has declined by 40% (Hobbs and Stoops 2002), with past rebuilding efforts focused only on the downtown district (Ryan 2008) and current efforts focused on only a subset of neighborhoods (MacDonald 2011).

b. Metrics of comparability

This study integrated multiple observation networks into a single network. The standard observations managed by the NWS were used as this network's baseline. To this baseline, observations were added from both an existing network run by the Michigan Department of Environmental Quality (MDEQ) and a temporary network that was established for this study. The temporary network ran for the length of this study and consisted of only the 110 days from 13 June to 30 September 2009. These networks, the data used, and the work undertaken to homogenize them are described in detail in the appendix. In addition to the observational network data, the hourly 2-m temperature and dewpoint temperature recorded at Detroit Metropolitan Airport (KDTW; Mannarano 1998) from 1979 through 2009 was acquired from the National Climatic Data Center (NCDC; National Climatic Data Center 2010).

Complications arise when integrating multiple networks; each network has unique monitoring uncertainties and also further uncertainties arise when using them in concert. The appendix describes in detail how the uncertainties associated with each network's observations are derived. A metric of comparison was desired that would allow for comparison of values across the network but would also ensure that any spatial variability found would exceed the uncertainty of the networks. This new-formed metric is herein referred to as the "spatial anomaly" and is defined mathematically as

$$\text{spatial\_anomaly}_{i,j,d} \equiv (T_{i,j,d} - \overline{T_{j,d}}) \pm \text{uncert}_{i,j} \begin{cases} +, (T_{i,j,d} - \overline{T_{j,d}}) < 0 \\ -, (T_{i,j,d} - \overline{T_{j,d}}) > 0 \end{cases},$$

with d being the day, j signifying either daily high or low, and i indicating location. First, the differences between each day's value $T_{i,j,d}$ of the daily high (or low) at each location and the network mean (i.e., across all sensors) of that particular daily high or low $\overline{T_{j,d}}$ were calculated. Then, depending on the sign of the first term $(T_{i,j,d} - \overline{T_{j,d}})$, the network-specific uncertainty value $\text{uncert}_{i,j}$ was either subtracted or added in a manner that always worked to reduce the absolute value of the first term (as indicated by the rules to the right of the curly brace).

The network used in this study lacked true representation of the rural surroundings (Fig. 1). Therefore this study could only assess the spatial variability throughout the urban and suburban regions of Detroit. This variability is herein referred to as the intraurban/suburban spatial variability in temperature (IUSSVT). In informally applying Oke's system of urban climate zones (Oke 2004), it is seen that the sites spanned all zones except the downtown tall-building zone (i.e., urban climate zone 1). The IUSSVT was quantified by calculating the range of the simultaneously (across all monitors in the network) observed spatial anomalies [herein referred to as the *range of simultaneously observed spatial anomalies* (*SOSAs*)]. The range of SOSAs is similar to the common metrics *UHI magnitude* and *UHI intensity* that are the temperature differences between urban and rural locations; in this case, however, the range of SOSAs only quantifies the range in temperatures across the urban and suburban landscape. At night the range of SOSAs is similar to the UHI-magnitude metric but likely underestimates it. During the daytime the range of SOSAs allows a positive value even if the downtown area is cooler than the suburban areas (commonly known as an urban cool island). Therefore knowledge of the typical spatial pattern of temperature is crucial when using the range-of-SOSAs metric. In addition, the metrics *intraurban heat island intensity* (Eliasson 1996; Erell and Williamson 2007; Yokobori and Ohta 2009) and *intraurban* and *intrasuburban spatial variability in temperatures* (Basara et al. 2008) are

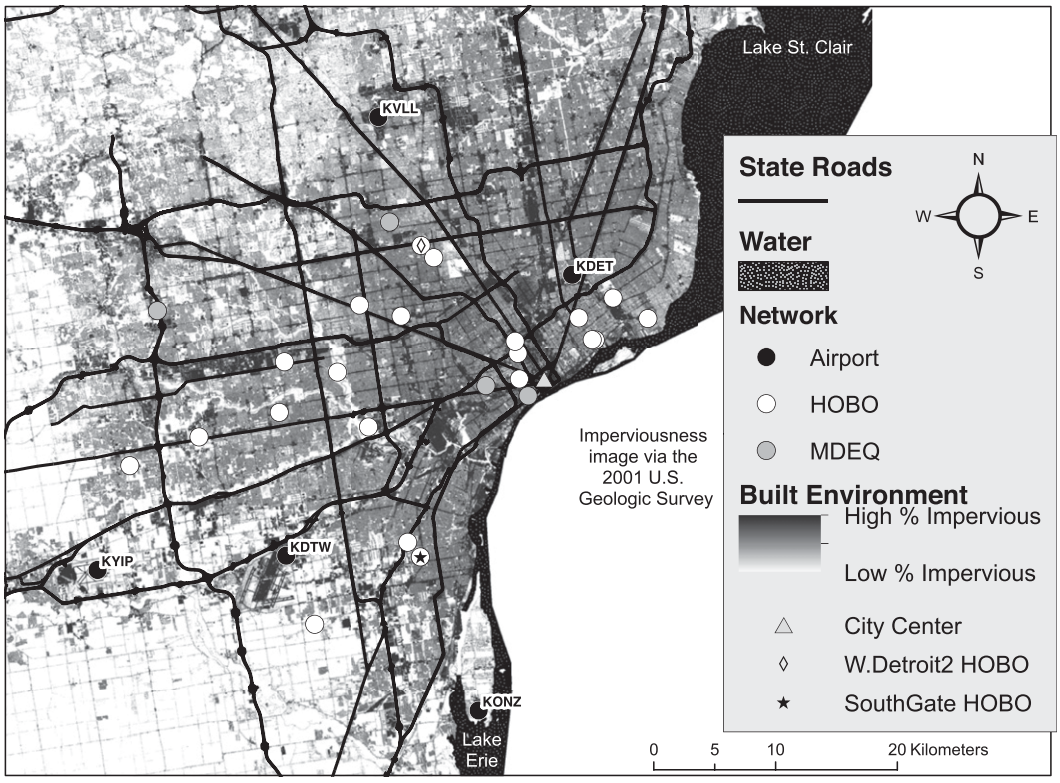

FIG. 1. Combined observational network in Detroit during the 2009 study, superimposed over a map of the area that shows impervious surface as captured by satellite imagery. Only western portions of the lakes are shown.

different from the range-of-SOSAs metric. These three metrics would be problematic in Detroit because the water bodies likely create large variability among similarly classified (e.g., suburban) locations. In addition, because it was unclear where to draw the distinction between urban, suburban, and rural/open locations (Peterson and Owen 2005), this study does not rigorously classify locations as such. The intraurban heat island metric *difference between urban canyon and suburban* value is likely larger than the range of SOSAs, because this study has no sites within a canyonlike environment. The intraurban and intrasuburban metrics likely have smaller values than the range-of-SOSAs metric because they are restricted to either the urban or suburban domains. The range of SOSAs was subsequently calculated for each day in the study, separately for both daily high and low.

c. *General characterization of the IUSSVT and summer 2009*

The histograms and the maximum and mean values of the range of SOSAs, of both daily extremes, were calculated during the study period. Student's *t* tests were performed to confirm that the mean range of SOSAs was larger than zero at the 5% significance level. Next, the Spearman rank correlation coefficients *r* and significance values *p* (Spearman 1907) were calculated between the ranges of SOSAs and both mean cloud-cover percentages and wind speeds (at 10 m). Nonparametric correlations were used throughout this study because of their robustness to departures from normality in data distributions. For this correlation, we chose to spatially average wind speed and cloud cover across three surrounding airports (KVLL, KDET, and KDTW; see Fig. 1) and temporally average for the morning between 0400 and 0800 eastern daylight time (EDT; UTC − 4 h) and for the afternoon between 1400 and 1800 EDT. Overnight wind speed, overnight cloud cover, and the previous-afternoon cloud cover were the variables that were correlated with the daily low ranges of SOSAs; the daily high variables were afternoon cloud cover and afternoon wind speed.

Next the temporal averages were assessed. The average of the spatial anomalies over the duration of the field study (110 days) was calculated for all locations and is referred to as the mean spatial anomaly. The spatial pattern of the mean spatial anomalies was displayed by plotting them on a map, and then the range of these spatial anomalies was calculated. To quantify the consistency in the spatial pattern of spatial anomalies, the range in the mean spatial anomalies was compared with

the mean range of SOSAs. We suggest a smaller range in the mean spatial anomalies is caused by a lack of consistency. We were, however, unable to find this method of assessing spatial consistency used previously in the urban-climate or pollution-monitoring literature.

A weeklong high pressure system from 31 August to 6 September 2009 had weather conditions that were highly conducive (i.e., low wind speeds and clear skies; Bonan 2008) to the influence of the urban landscape. This period was analyzed separately so that the IUSSVT during high pressure systems could be compared with the 110-day mean IUSSVT. To do so, the mean range of SOSAs during the period of the high pressure system was calculated and was compared with its 110-day-derived counterparts. In another effort to assess the consistency of the spatial pattern, the averaged high pressure system spatial anomalies were correlated with similar values derived from all available days not included in this week (103 days) in a way that is similar to another study (Finkelstein and Jerrett 2007).

To quantify how stressful the weather was relative to long-term summer weather data, the 2009 temperature data were compared with the 30 years of data observed at KDTW. Apparent temperatures (Steadman 1984), rather than conventional air temperatures, were used for this comparison because this region often has high levels of water vapor. For each day during the observational period, both the maximum afternoon daily high and minimum morning daily low apparent temperatures were calculated, using temperature and water vapor content. The percentile for each day during the observational period was subsequently determined, for both daily extremes, using the past 30 years of apparent temperatures experienced in Detroit on that date. This allowed us to use a heat-event definition that is based on climatological percentiles, to quantify both daily extremes' percentiles for each day, and then to calculate the study-period average percentiles.

Next, the existence of IUSSVT during weather conditions that were objectively classified as stressful in terms of heat was investigated. First, days were identified that could be classified as either heat events or ''oppressive,'' as defined by either a climatologically based or an airmass-based definition. In general, such methods characterize days as oppressive if the weather conditions result in high heat stress, and if the conditions are sustained it is termed a heat event. The climatologically based definition, described by Easterling et al. (2007), requires three days with the daily high exceeding the 80th percentile of daily highs for that day and subsequent daily lows exceeding the 80th percentile of lows for that day. Once such heat events were determined during the study period, the mean range of SOSAs was calculated during those periods. Then Student's t tests were performed to confirm that the sample means were greater than zero at the 5% significance level. If no heat events existed according to that definition, then the individual days indicated as oppressive were analyzed as a group. In addition, any heat events or individual oppressive days, as indicated by the airmass-based Spatial Synoptic Classification 2 (SSC2) (Sheridan 2002; Kalkstein and Sheridan 2003) system, were examined in the same manner. The calendar data provided by Dr. S. Sheridan's website (Sheridan 2010) were used for this purpose.

d. Correlation with land-cover and location attributes

The intraurban/suburban temperature pattern was modeled statistically using land-cover and location information. First the relevant land-cover and location variables were proposed and created. Then correlations between the different land-cover and location variables and the mean spatial anomalies at each station were calculated. Then multiple-variable regression equations were created, evaluated for goodness, and validated. This method is similar to the land-use regression common in the literature on air-pollution exposure (Hoek et al. 2008).

The first variable, percent of impervious surface, is an indicator of the built environment (Oke 1982; Arnold and Gibbons 1996). Impervious surfaces were identified from Landsat imagery, taken in 2001 (U.S. Geological Survey 2008), as the hard constructed surfaces that cover buildings, roadways, parking lots, and so on. Areas with more impervious surface are more likely to store heat and then release that heat overnight. Imperviousness does not take into account the three-dimensional geometrical factors or distance from city center. Maps were constructed with both the sites of the networks and superimposed satellite-image-based measurements that characterized the imperviousness. Using ArcGIS proprietary software (ESRI Corporation of Redlands, California), the percent of surrounding surface indicated as impervious was calculated for each station. To determine the strongest relationship between values of percent of impervious surface and both daily extremes, the correlation coefficients were repeatedly calculated between the station's mean spatial anomalies, both highs and lows, and the values of percent of impervious surface within various circular radii from 0.2 to 3.0 km. The rest of the assessment then moved forward with those radii of strongest correlation.

The next variable investigated was proximity to a significant water body. In theory, both local lake breezes and synoptic cold-air advection can cool the nearshore regions during the daily highs. As well, the higher thermal inertia of a water body should dampen

the diurnal cycle and affect both daily extremes. Straight-line distances to a sizeable water body at each station were calculated in ArcGIS, and the correlations between those values and both extreme's mean spatial anomalies were calculated.

Last, distance from city center was examined for correlation with the intraurban/suburban temperature pattern. In theory, daily highs might be warmer at the city center because of increased anthropogenic heat flux and roughness length at the city center, and the latent heat flux and shortwave albedo should be lowest in the city's interior. One can make the case for a cooler downtown in Detroit during the daily high, however, given the water bodies' close proximity (Fig. 1). As an alternative, the relationship between the daily lows and distance from city center is straightforward, given that anthropogenic heat flux, urban-canyon effect and volumetric heat capacity are all expected to be largest at the city center. Straight-line distances from the western side of the downtown district (Fig. 1) to each station were calculated in ArcGIS, and the correlations between those values and both daily extreme's mean spatial anomalies were calculated.

Stepwise regression using the backward-elimination method (Draper and Smith 1981) was employed with the aforementioned land-cover and location variables, per daily extreme, to create a regression model that predicted the mean spatial anomalies. The regression assumptions that the residuals have a normal distribution and constant variance were confirmed in each model (results not shown). Calculation of the coefficient of determination R^2, the full-model p value, and the root-mean-square error (RMSE) allowed for evaluation of the model goodness of fit (Draper and Smith 1981). Last, validation of the models was done using the leave-one-out cross-validation method (Hoek et al. 2008), in which the model is developed on the basis of $n - 1$ stations and the predicted value at the location of the left-out station is compared with the actual measured value at that station. This procedure was repeated n times, and the mean RMSE between the predicted and observed spatial anomalies, across all sites, was then calculated and was compared with the RMSE of the model fit to data from all of the stations.

3. Results

a. Summer of 2009 climatological behavior

Each day's percentile of apparent temperature at KDTW was calculated for both daily extremes. Both were slightly cooler than climatic normal, with the average lows and highs at the 47th and 43rd percentiles, respectively. (The daily climate percentiles as a function of time, for both daily extremes and over the 110 days, are available as supplemental material Fig. S1 at the Journals Online website: http://dx.doi.org/10.1175/JAMC-D-11-0127.s1.)

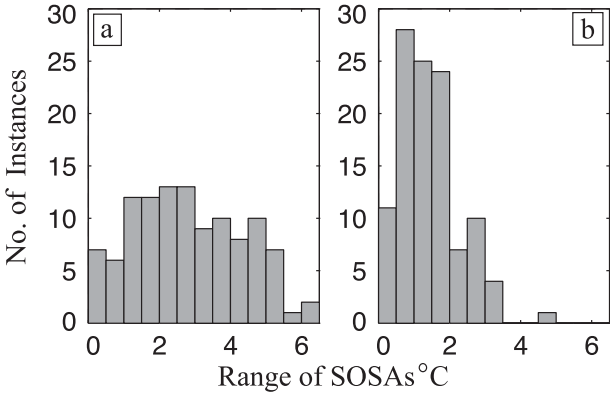

FIG. 2. Histograms of observed range of SOSAs during the experiment for (a) daily low and (b) daily high temperature extremes. Sample size for both is 110 days.

b. General characterization of the IUSSVT

The histograms of the daily high and low range of SOSAs during the observational period (Fig. 2) show that the two distributions were noticeably different, with the daily highs being right skewed. The largest individual ranges of SOSAs of the daily high and low temperatures were 4.8° and 6.3°C, respectively. The mean range of SOSAs was 1.4°C in the daily highs and 2.8°C in the lows. For both daily extremes, a Student's t test rejected the null hypothesis that either of the true mean range of SOSAs could be zero.

The correlation coefficients that were calculated between each day's range of SOSAs and mean morning wind speeds ($r = -0.60$; $p < 0.001$), cloud-cover percentage ($r = -0.67$; $p < 0.001$), and previous-afternoon cloud-cover percentage ($r = -0.45$; $p < 0.001$) were all both significant and negative (Fig. 3). For the daily high ranges of SOSAs, however, a significant and negative correlation coefficient was found with mean afternoon wind speeds ($r = -0.40$; $p < 0.001$) but not with cloud cover ($r = 0.07$; $p = 0.47$).

The differences between daily highs and lows are also evident in the temporal averages. The spatial pattern of both the mean spatial anomalies were calculated and plotted on a map of Detroit (Fig. 4). The range of these mean spatial anomalies was 2.0°C in the daily lows (72% of the mean range of SOSAs), but the daily high range of the mean spatial anomalies was only 0.6°C (42% of its respective mean range of SOSAs).

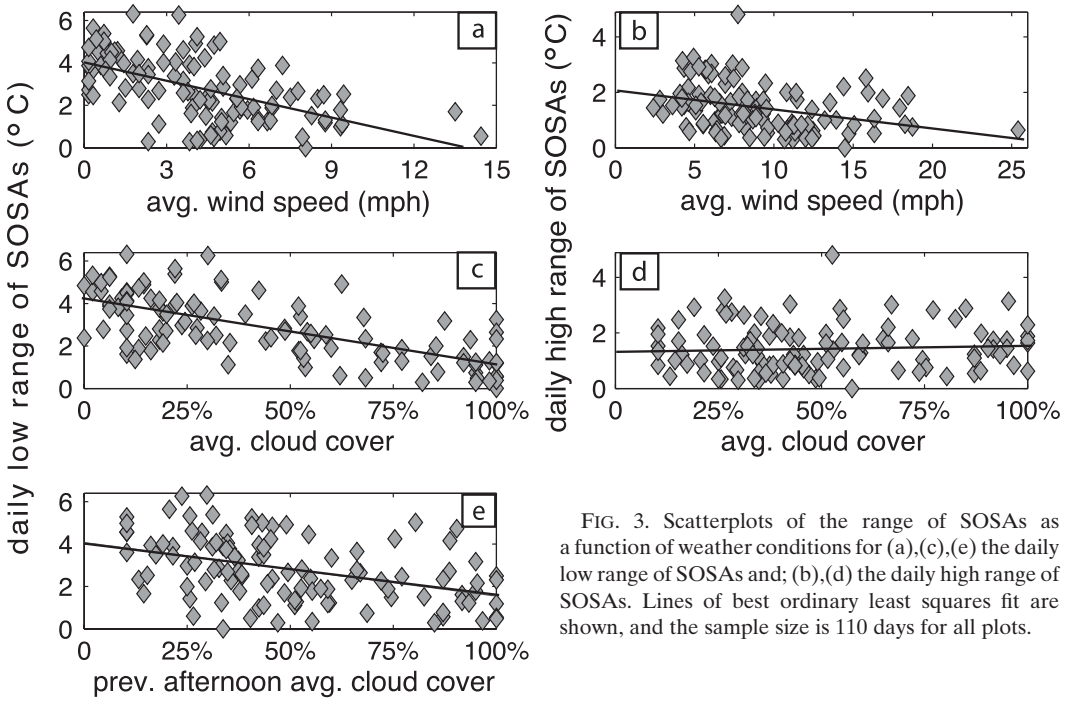

FIG. 3. Scatterplots of the range of SOSAs as a function of weather conditions for (a),(c),(e) the daily low range of SOSAs and; (b),(d) the daily high range of SOSAs. Lines of best ordinary least squares fit are shown, and the sample size is 110 days for all plots.

During a weeklong high pressure system, each station's spatial anomaly was temporally averaged. The range in the daily low mean spatial anomalies was 4.1°C, and the range was 1.3°C in the daily highs. The mean range of SOSAs in the daily lows was 4.3°C, and the mean range of SOSAs in daily highs was only 1.9°C. A comparison of the values observed during the high pressure system with 110-day mean derived values showed that the 110-day mean range of SOSAs was 65% of the high pressure mean range of SOSAs during the daily lows and 74% during the daily highs. The correlation coefficients calculated between the high pressure system mean spatial anomalies and the average spatial anomalies derived from all the other days was 0.88 in the daily lows and 0.63 in the daily highs.

There was a heat event according to the Easterling et al. definition on 21, 22, and 23 September 2009. During this period the mean range of SOSAs was 0.6°C during the nightly lows and 1.1°C during the daily highs. Student's *t* tests could not reject the null hypotheses that the true mean ranges in SOSAs could be zero for either daily extreme, however—possibly because of the small

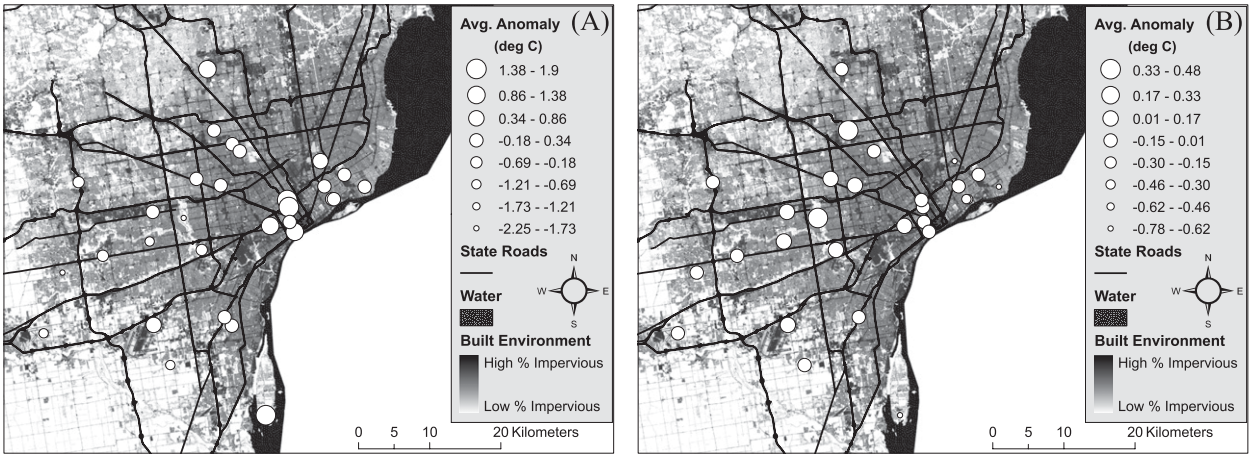

FIG. 4. Observed mean spatial anomalies over the duration of the observational period. Spatial anomalies shown are the means from all 110 observations between 13 Jun and 30 Sep for both (a) daily low and (b) daily high temperature extremes. Circle sizes coordinate with eight equal-interval groupings; the ranges vary between the two figures.

TABLE 1. Spearman rank correlation coefficients (with p values in parentheses) between land-cover and location variables and both 110-day mean spatial anomalies and other variables. SAI_0.2 km = percent of impervious surface within a 0.2-km radius, SAI_1.95 km = percent of impervious surface within a 1.95-km radius, H2O_dist = straight-line distance to large water body, and CC_dist = straight-line distance to city center.

Field	SAI_0.2 km	SAI_1.95 km	H2O_dist	CC_dist
Low spatial anomalies	0.68 (<0.001)	0.27 (0.15)	−0.52 (<0.01)	−0.45 (0.014)
High spatial anomalies	0.11 (0.57)	0.39 (0.04)	0.50 (<0.01)	0.21 (0.28)
SAI_0.2 km	1 (0)	0.47 (<0.01)	−0.30 (0.11)	−0.60 (<0.001)
SAI_1.95 km	0.47 (<0.01)	1 (0)	−0.12 (0.54)	−0.65 (<0.001)
H2O_dist	−0.30 (0.11)	−0.12 (0.54)	1 (0)	0.74 (<0.001)

sample size. Then, any daily extreme meeting the 80th percentile criterion was considered (n = 19 for lows; n = 12 for highs). The recalculated mean range of SOSAs was 2.2°C in the lows and 1.6°C in the daily highs. With this larger sample size, the Student's t tests for both daily extremes rejected the null hypothesis that the true mean ranges in SOSAs could be zero. The SSC2 method did not indicate any consecutive days with oppressive weather during the study; hence, there were no heat events. Instead all days classified as oppressive-type air masses (''dry tropical,'' ''moist tropical +,'' and ''moist tropical ++''; Kalkstein and Sheridan 2003) were grouped together (n = 3), and the mean ranges in SOSAs in both the daily lows and highs were calculated at 2.0° and 0.9°C, respectively. Student's t tests for both daily extremes during those three days could not reject the null hypothesis that the true mean ranges in SOSAs could be zero.

c. *Correlation with land-cover attributes*

The strongest correlations between the mean spatial anomalies and percent impervious surface values were with the 0.2-km radius in daily lows and with the 1.95-km radius for the daily highs. (The correlation coefficients as a function of radius, for both daily extremes, are available as supplemental material Fig. S2 at the Journals Online website: http://dx.doi.org/10.1175/JAMC-D-11-0127.s2.) The correlation coefficient between the mean daily low spatial anomalies and the values of 0.2-km-radius percent of impervious surface was much larger than the correlation coefficient between the mean daily high spatial anomalies and the values of percent of impervious surface at the 1.95-km radius (Table 1; Fig. 5).

The correlations between proximity to water and both the mean daily high and low spatial anomalies were found to be similar and significant but with different signs (Table 1; Fig. 5). It was also noted that the correlations between the proximity to water values and both values of percent of impervious surface were without significance at both distances (Table 1).

Proximity to the city's center showed relatively weak correlations with both the mean daily highs and lows (Fig. 5). The correlation with the mean daily low spatial anomalies was significant and negative but with less significance than that with the values of 0.2-km percent of impervious surface (Table 1). The daily highs were not a significant function of proximity to city center (Table 1). The usefulness of this variable as a predictor was further limited by strong correlations with the other land-cover and location variables (Table 1).

The stepwise-regression backward-elimination method resulted in including all three land-cover and location variables in the daily low regression model. The coefficients of the normalized variables indicated that percent of impervious surface was significantly more influential than the other two variables (Table 2). The RMSE for this model was calculated at 0.3°C (as compared with the range in mean spatial anomalies, which was 2.0°C), the R^2 was 0.62, and the p value was on the order of 10^{-5}. Model validation results from the cross-validation method of an RMSE of 0.4°C were comparable to the RMSE of the full model.

For the daily high regression model, the backward-elimination method indicated that the distance-to-city-center and proximity-to-water variables were the appropriate predictor land-cover and location variables. The coefficients of the normalized predictor variables suggested similar influence from both variables. This model led to an RMSE of 0.1°C (as compared with, the range in mean spatial anomalies, which was 0.6°C), an R^2 of 0.33, and a p value on the order of 10^{-3}. These results indicated an unsatisfying model (RMSE of ~17% of range), and thus further validation was not undertaken.

4. Discussion

a. *Spatial variability in comparison with previous studies*

IUSSVT was more prominent in the study area/period during the daily lows than during the highs, based on the calculated means and histograms of the observed ranges of SOSAs. This is similar to other recent studies that

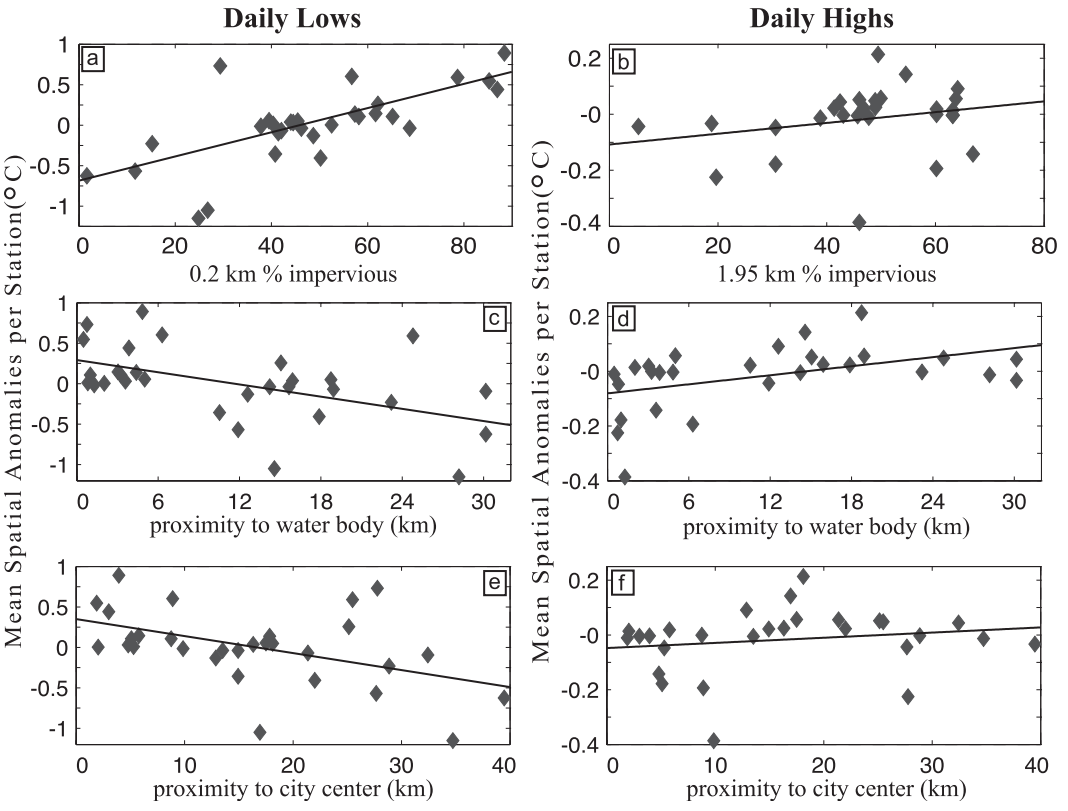

FIG. 5. Scatterplots of temperature observations as a function of three land-cover and location attributes. Spatial anomalies are averaged over the study's 110-day duration. The sample size is 30 and 28 for daily low and highs, respectively. Also shown are lines of ordinary least squares fit.

found both the UHI magnitude (Runnalls and Oke 2000; Wilby 2003; Erell and Williamson 2007; Gaffin et al. 2008; Basara et al. 2008; Camilloni and Barrucand 2012) and intraurban spatial variability (Wilby 2003; Erell and Williamson 2007; Gaffin et al. 2008; Basara et al. 2008) to be largest at nighttime. Similar to findings in Oklahoma City in 2003 (Basara et al. 2008), our results also show an amount of IUSSVT also existed during the daily high.

The correlation coefficients calculated between the amount of IUSSVT and wind speeds and cloud cover indicated that IUSSVT is strongly controlled by the larger-scale weather conditions. This is consistent with other recent studies that indicated both nighttime intraurban spatial variability (Eliasson 1996; Wilby 2003; Kim and Baik 2005; Erell and Williamson 2007) and UHI magnitude (Runnalls and Oke 2000; Morris et al. 2001; Gedzelman et al. 2003; Wilby 2003; Camilloni and Barrucand 2012) to be largest during weather conditions of low wind speed and clear sky. Our results elaborate on these findings by suggesting an explicit relationship between daily low IUSSVT and the previous afternoon's average cloud cover that was not readily found in the literature.

Greater consistency in the spatial pattern of temperature during the daily lows than during the daily highs was indicated both by comparison between the daily high and low ratios (of range in mean spatial anomalies to the mean range in spatial anomalies), and by comparison of the correlation coefficients between the average spatial anomalies derived from a weeklong high pressure system and the rest of the study. We concluded that the daily high IUSSVT consisted primarily of spatial noise whereas the daily low IUSSVT manifested itself in a more consistent

TABLE 2. Regression coefficients of the predictor variables within the statistical models predicting the observed mean spatial anomalies. Const = y-intercept value (°C), SAI_0.2 km = the percent of impervious surface at the 0.2-km radius, H2O_dist = the straight-line distance to large water body (km), and CC_dist = straight-line distance to city center (km). Normalized indicates with normalized predictor variables.

Field	Daily low	(Normalized)	Daily high	(Normalized)
Const	−0.9144	−0.9144	−0.0423	−0.0423
SAI_0.2 km	0.0177	0.3762	—	—
H2O_dist	−0.0314	−0.2965	0.0121	0.1169
CC_dist	0.0257	0.2696	−0.0071	−0.0767

spatial pattern. In the literature there is a relative lack of comparable assessments of the consistency of intraurban or intrasuburban spatial patterns.

b. Spatial variability exists, even during hot weather

A nonzero amount of IUSSVT exists across the Detroit region on average during the summer, and the statistical tests confirmed that. This mirrors the conclusions of many other studies (Saaroni et al. 2000; Hart and Sailor 2009; Basara et al. 2008; Bottyán and Unger 2003; Yokobori and Ohta 2009) that showed that significant intraurban variability in temperatures exists. IUSSVT, particularly in the daily lows, was larger than average during high pressure conditions—shown by calculating and comparing metrics during a weeklong high pressure period. This conclusion complements results from other studies that have explicitly shown the UHI magnitude to be large during high pressure (Wilby 2003; Yagüe et al. 1991).

The results suggested that during weather of high heat stress the IUSSVT still existed. The mean range of SOSAs calculated during hot weather was comparable to the temporal average, and statistical test results indicated the true mean range of SOSAs during hot weather was not zero. Previous studies (Hajat and Kosatky 2010) have documented the public-health significance of even a 1°C change in temperature during hot temperature (1%–3% increase in mortality risk); the mean range of SOSAs observed during hot weather was comparable to that and thus can be seen as significant. Very few studies have investigated this aspect, but our results confirm the findings of a previous study (Basara et al. 2010) that examined both the intraurban and intrasuburban temperature variability during a heat event.

c. Predicting the intraurban/suburban spatial pattern of temperature

The daily low, but not daily high, mean spatial intraurban/suburban temperature pattern could be explained by relevant land-cover and location information as indicated by model diagnostics. All three land-cover and location variables were found to be significant in a statistical model of the daily low mean spatial anomalies. Similar studies using statistical models to statistically explain the nighttime intraurban/suburban spatial pattern of temperature (Kuttler et al. 1996; Bottyán and Unger 2003; Buttstädt et al. 2010) confirmed it could be done well (R^2 between 0.50 and 0.85) and with only a small number of variables (2–4). Other studies (Gaffin et al. 2008), however, failed to find land-cover variables driving temperature but did not use the same variables that this study did.

The daily low regression model produced adequate cross-validation results. Percent of impervious surface was the most influential predictor, even over the more-traditional distance-to-city-center variable (Table 1), and we suggest future studies attempt to include it in similar statistical models. Regression results also confirmed the significance (both day and night) of distance to water as a predictor (Table 1), and this was reminiscent of similar conclusions in two nearby cities: Chicago (Ackerman 1985) and Toronto, Canada (Mohsin and Gough 2012). This model is specific to the context of Detroit and therefore is unlikely to be useful in predicting the intraurban/suburban spatial patterns of temperature in other cities.

d. Implications for public-health officials

This study's results suggest that officials in charge of reducing heat-related mortality and morbidity should be aware of relevant IUSSVT across the Detroit region during hot weather. Officials in charge of protecting the public should be aware that the IUSSVT is likely more significant when the weather consists of calm winds and clear skies (e.g., during a high pressure system). Detroit's intraurban/suburban spatial temperature patterns of daily highs and lows could lead to differing temperature exposures to people, depending on their physical location in the area, even on the same day and at the same time. Thus, these patterns are an important component in vulnerability mapping and should be relevant in the decision of where to focus heat-adaptation strategies (Wilhelmi et al. 2004). For example, since the IUSSVT is most relevant during the daily low, the results (Fig. 4) suggest focusing heat-adaptation efforts (e.g., community buddy systems, flyers and neighborhood meetings, and reducing the amount of impervious surfaces in neighborhoods) downtown and on the east side of the city. The results (Fig. 4) also suggest that strategies that are focused primarily on reducing exposures to daily high temperatures, such as opening cooling centers/community pools, planting trees, and increasing albedo, would be most effectively implemented on the west side of Detroit.

Acknowledgments. The research was sponsored by the Graham Environmental Sustainability Institute at the University of Michigan, the U.S. Environmental Protection Agency Science to Achieve Results (STAR) under Grant R832752010, the Centers for Disease Control and Prevention under Grant R18EH000348, and the Great Lakes Integrated Sciences and Assessments Center (GLISA) Climate Program Office Grant NA10OAR4310213. This is contribution 2012-1 of GLISA. We also appreciate Craig Fitzner (MDEQ) for providing scientific data support.

APPENDIX

Integrating Multiple Observation Networks into a Single Network

For this study it was chosen to integrate multiple networks into one observing network. Although it was not the focus of this study, future studies might also construct such networks. In the following text, first the networks and data used are described and then comparability between the networks and uncertainty in using the network are explained.

a. NWS network

The standard observations used were observed at the local airports by the NWS's Automated Weather Observing Station (AWOS) and Automated Surface Observing Station (ASOS) networks (Mannarano 1998). Temperature measurements are observed at a 1.5-m height. These are the standard operational products used by the weather service and are subject to calibration standards (Mannarano 1998). Five airports, located primarily on the outskirts of the city, were used in the network (Fig. 1). The hourly temperature, cloud cover, and wind speed [taken at 10 m above ground level (AGL)] data during the observational period were acquired from the NCDC.

b. The MDEQ network

The MDEQ operates an air-pollution-monitoring network as mandated by the U.S. Environmental Protection Agency for monitoring compliance with National Ambient Air Quality Standards under the Clean Air Act (Department of Natural Resources and Environment 2010). This network provided hourly means of air temperatures at 5 m AGL (i.e., still within the urban canopy layer) and wind characteristics measured at 10 m AGL. Six of their monitoring locations were suitable for this study, and the aforementioned data were acquired through contact with the MDEQ staff.

c. The temporarily established network

For the custom study network, 21 ''U23-002 HOBO Pro V2 External Temperature/RH'' dataloggers from the Onset Computer Corporation (Pocasset, Massachusetts) were used, herein referred to as HOBOs. Logger specifications can be examined online (http://www.microdaq.com/occ/u23/external_temp_rh_data_logger.php#specs). Previous studies have demonstrated that these monitors are capable of detailed studies of the spatial structure of temperature fields (Whiteman et al. 2000). The HOBO monitors consist of temperature and relative humidity sensors inside naturally aspirated radiation shields and are fastened to thin wooden stakes, along with a datalogger, at a height of 1.5 m AGL. Detroit-area residents were approached for permission to place loggers outside their homes, which ranged in location from the city limits to the old downtown district; near and far from the two lakes (Erie and St. Clair) and the Detroit River; in densely populated suburbs to the outskirts of more distant suburban communities; and on a sizeable island (Fig. 1). To the east of the Detroit River lies the city of Windsor, Ontario, Canada; it was assumed that Windsor's close proximity did not affect Detroit's temperature pattern because it is typically downwind of Detroit and is separated from Detroit by a river that is up to 4 km in width. The HOBOs were placed primarily in backyards of participants, sampling at a 10-min frequency, and sited to minimize microclimate impacts (e.g., over grassy groundcover, ample sky view, and away from heat sources). In addition, it was assumed that the turbulent mixing produced by flow around barriers was adequate to blend the observed atmospheric temperatures so as to allow measurement of local-scale average temperatures.

d. Evaluating comparability of the networks

A primary advantage of the HOBO network was the ability to calibrate its measurements with those of existing networks. In general, the method for a given calibration period was 1) to locate a HOBO monitor in as close proximity as possible to at least one monitor from an existing network, 2) to quantify the relationship, or *bias*, between the co-observed daily temperature extremes, 3) if necessary, to apply bias corrections or simple modeling to make observations as similar as possible, and then 4) to requantify the mean difference between HOBO and existing network observations over the calibration experiment, referred to as the *uncertainty* (Table A1) in using the existing network with the HOBO network.

First the accuracy of the HOBO monitors relative to one another was empirically determined. Postdeployment tests were chosen because they would capture any drift in accuracy of the monitors during the field study. All monitors were placed in a temperature-controlled room during testing. With 3097 measurements per monitor, a mean instantaneous range of 0.44°C was calculated. This is referred to as the ''inherent-relative uncertainty'' of the HOBO network (Table A1).

Then the differences between the HOBO network and the standard NWS observations from the airports were sought. Although it was impossible to gain permission to collocate monitors on airport property, a monitor was located 2.7 km away from one of the airport monitoring locations (KDTW), and the differences

TABLE A1. Determined biases and uncertainties between networks (°C). Footnote abbreviations: HOBO_t = HOBO temperature extreme observation (°C), MDEQ_t = MDEQ temperature extreme observation (°C), avg_WS = MDEQ stations mean observed wind speed (m s^{-1}) between 0300 and 0800 EDT or between 1400 and 1800 EDT, and CC% = mean airport observed cloud-cover percentage between 0400 and 0800 EDT or between 1300 and 1800 EDT.

Network and difference	Bias	Uncertainty
Daily low		
Airport instrumentation	—	0.5
HOBO inherent-relative	—	0.44
HOBO microclimate	—	0.0
HOBO siting	+0.14	0.0
HOBO sampling algorithm	+0.16	0.11
MDEQ collocation	*	0.43
MDEQ sampling algorithm	+0.16	0.11
Daily high		
Airport instrumentation	—	0.5
HOBO inherent-relative	—	0.44
HOBO microclimate	—	0.32
HOBO siting	+0.49	0.0
HOBO sampling algorithm	−0.48	0.28
MDEQ collocation	**	0.52
MDEQ sampling algorithm	−0.48	0.28

* HOBO_t ≈ −4.2 + 1.1 × MDEQ_t + 0.13 × avg_WS − 2.0 × (1 − CC%).

** HOBO_t ≈ 5.8 + 0.97 × MDEQ_t − 0.16 × avg_WS + 1.3 × (1 − CC%).

were observed for 2 weeks. This large distance and small sample size is a limitation to the network calibration. As a consequence, the siting and sampling algorithm differences were accounted for separately. This HOBO siting was typical of the other HOBO monitor sitings as opposed to the very open airport monitor sitings. Using the nearby HOBO monitor observations, which sampled at a higher frequency (2 min) than the typical HOBO monitor, the KDTW observations (i.e., mean value within 5 min prior to the hour) were replicated, and the mean bias for the daily minimum and maximum temperatures was calculated at +0.14°C and +0.49°C, respectively. Once the HOBO observations were adjusted for this bias, both daily high and low mean differences were calculated at less than the 0.5°C prescribed uncertainty of the ASOS/AWOS instrumentation; therefore 0.0°C was adopted as the ''HOBO siting uncertainty'' (Table A1). When using the NWS AWOS/ASOS observations in the network, however, it was assumed that they have a 0.5°C ''instrumentation uncertainty'' (Table A1).

The temporal sampling varies across the networks. For this study the daily lows were taken as the minimum temperature recorded between 0100 and 0700 EDT, and the daily highs were taken as the maximum temperature recorded between 1300 and 1900 EDT. The HOBO monitors are programmable, but the typical configuration was a 10-min sampling frequency with no additional averaging. The MDEQ network reports hourly means every hour, and the airport network reports 5-min means every hour. To test the impact of the temporal sampling differences, a HOBO was set to sample on a 1-min sampling frequency over the duration of the study and was used to replicate the various network products each day. This was used to estimate the biases and uncertainties associated with the different temporal sampling algorithms among the networks.

The HOBO–AWOS/ASOS collocation experiment was only 2 weeks long, and so it was elected to explicitly account for the difference in sampling algorithms. This bias between AWOS/ASOS and HOBO observations was calculated at −0.48°C for the daily high and +0.16°C for the daily lows. The mean difference, after these bias corrections were applied, was calculated at 0.28°C for the daily highs and 0.11°C for the daily lows, and this is referred to as the ''HOBO sampling algorithm uncertainty'' (Table A1). Because the HOBO–MDEQ collocation experiment occurred over a large sample, we decided to incorporate the sampling-algorithm difference between the two networks in the collocation experiment. Thus it was still necessary to use the HOBO–AWOS/ASOS sampling-algorithm bias and uncertainty values, since the airport sampling—and not the HOBO sampling—was the baseline.

To combine data from the MDEQ network, quantification was needed of the differences in observations that were due to the differences in height, instrumentation, and sampling algorithm between the network's measurements and HOBO observations. To quantify the sum impact of these differences, two 1.5-m AGL HOBO monitors were collocated (approximately 20-m horizontal separations) at two MDEQ monitoring sites for 2 months. On-site MDEQ wind speed and nearest-airport sky-cover observations were useful in predicting the daily extreme HOBO observations from MDEQ observations. The relationship discovered was designed to be non-site-specific by pooling the data from both collocation sites for the 2-month duration (128 days in total) and then building the relationships. The linear multiple-regression equations used for this prediction are briefly provided (Table A1), and analysis of fit was performed (results not shown). The mean differences between MDEQ-predicted and HOBO-observed extremes were adopted as the ''MDEQ collocation uncertainty'' (Table A1) and were calculated at 0.43° and 0.52°C, for the daily lows and highs, respectively. The measurement uncertainty stated in the MDEQ instrumentation specifications was 0.3°C, but

because this was less than the determined uncertainty it was assumed to be included in that value. Thus, the uncertainties were summed that were related to the collocation and sampling-algorithm differences. Summing these uncertainties resulted in an uncertainty in the daily lows of 0.54°C and in the daily highs of 0.80°C, when using the MDEQ stations observation with the larger network.

In addition, even with careful siting standards, inconsistency among HOBO observations was likely to exist, simply because they monitored in yards with different microclimates. It was decided not to include uncertainty arising from microclimate variability across both the six MDEQ stations and five AWOS/ASOS stations because we judged that the level of monitoring standardization and siting strictness was sufficient. To assess the magnitude of this uncertainty within the HOBO network, data from two similarly located and sited monitors (separated by ~300 m) were analyzed to determine the yard-to-yard differences, indicated in Table A1 as the "HOBO microclimate uncertainty." First the mean difference between the two monitors was calculated, over the duration of the study, per extreme, and showed a daily high value of 0.76°C and a daily low value of 0.33°C. For daily lows the inherent-relative uncertainty of the HOBO network was larger than this difference, and so the microclimate uncertainty was assumed to be 0°C. For daily highs the microclimate uncertainty exceeded the inherent-relative uncertainty by 0.32°C, however, and thus the daily high microclimate uncertainty was taken as 0.32°C. Therefore, for the final HOBO uncertainty calculation, all four uncertainties (inherent-relative, microclimate, siting, and sampling-algorithm difference) were summed, per daily extreme. This resulted in an assumed uncertainty in the daily lows of 0.55°C and in the daily highs of 1.04°C, when using HOBO values in the network.

Last, daily high measurements from two HOBO stations were excluded from the study. These stations were first identified as having possibly compromised sitings—to be more specific, a cement surface within 3 m of the monitor. These observations were subsequently compared with nearby observations to assess their quality. The morning lows showed no signs of siting impacts, consistent with tests (not shown) indicating undesirable microclimate characteristics to have a significantly lesser impact on daily low temperatures than on daily high temperatures. These stations were the Southgate and West Detroit No. 2 HOBO monitors (Fig. 1). All other monitors passed scrutiny of potentially compromised siting, so that the larger multinetwork network utilized a total of 30 and 28 stations for daily lows and highs, respectively. One station was located in a park that was roughly 1 km across, but we retained it within the network because we felt that it was not too large and was not particularly uncommon to cities.

REFERENCES

Ackerman, B., 1985: Temporal march of the Chicago heat island. *J. Climate Appl. Meteor.,* **24,** 547–554.

Arnold, C. L., and C. J. Gibbons, 1996: Impervious surface coverage: The emergence of a key environmental indicator. *J. Amer. Plann. Assoc.,* **62,** 243–258.

Basara, J. B., P. K. Hally Jr., A. J. Schroeder, B. G. Illston, and K. L. Nemunaitis, 2008: Diurnal cycle of the Oklahoma City urban heat island. *J. Geophys. Res.,* **113,** D20109, doi:10.1029/2008JD010311.

——, H. G. Basara, B. G. Illston, and K. C. Crawford, 2010: The impact of the urban heat island during an intense heat wave in Oklahoma City. *Adv. Meteor.,* **2010,** 230365, doi:10.1155/2010/230365.

Basu, R., 2009: High ambient temperature and mortality: A review of epidemiologic studies from 2001 to 2008. *Environ. Health,* **8,** 40, doi:10.1186/1476-069X-8-40.

Bonan, G., 2008: *Ecological Climatology: Concepts and Applications*. Cambridge University Press, 568 pp.

Bottyán, Z., and J. Unger, 2003: A multiple linear statistical model for estimating the mean maximum urban heat island. *Theor. Appl. Climatol.,* **75,** 233–243.

Buttstädt, M., T. Sachsen, G. Ketzler, H. Merbitz, and C. Schneider, 2010: Urban temperature distribution and detection of influencing factors in urban structure. *17th Conf. Int. Seminar on Urban Form,* Hamburg, Germany, University of Münster Institute of Comparative Urban History and University of Hamburg Institute of Geography, 17 pp. [Available online at http://www.isuf2010.de/Papers/Buttstaedt_Mareike.pdf.]

Camilloni, I., and M. Barrucand, 2012: Temporal variability of the Buenos Aires, Argentina, urban heat island. *Theor. Appl. Climatol.,* **107,** 47–58.

Davey, C. A., N. J. Doesken, R. J. Leffler, and R. A. Pielke, 2002: Differences between rooftop and standard ground-based temperature. Preprints, *Sixth Symp. on Integrated Observing System,* Orlando, FL, Amer. Meteor. Soc., 229–232.

Department of Natural Resources and Environment, cited 2010: Department of Environmental Quality: Monitoring. [Available online at http://www.michigan.gov/deq/0,1607,7-135-3310_4195—,00.html.]

Dole, R., and Coauthors, 2011: Was there a basis for anticipating the 2010 Russian heat wave? *Geophys. Res. Lett.,* **38,** L06702, doi:10.1029/2010GL046582.

Dolney, T. J., and S. C. Sheridan, 2006: The relationship between extreme heat and ambulance response calls for the city of Toronto, Ontario, Canada. *Environ. Res.,* **101,** 94–103.

Draper, N. S., and H. Smith, 1981: *Applied Regression Analysis*. John Wiley and Sons, 461 pp.

Easterling, D. R., B. Gleason, K. E. Kunkel, and R. J. Stouffer, 2007: A comparison of model produced climate extremes with observed and projected trends for the 20th and 21st centuries. *Extended Abstracts, AMS Forum: Climate Change Manifested by Changes in Weather,* San Antonio, TX, Amer. Meteor. Soc., 1.1. [Available online at http://ams.confex.com/ams/pdfpapers/116373.pdf.]

Eliasson, I., 1996: Intra-urban nocturnal temperature differences: A multivariate approach. *Climate Res.,* **7,** 21–30.

Erell, E., and T. Williamson, 2007: Intra-urban differences in canopy layer air temperature at a mid-latitude city. *Int. J. Climatol.,* **27,** 1243–1255.

Finkelstein, M. M., and M. Jerrett, 2007: A study of the relationships between Parkinson's disease and markers of traffic-derived and environmental manganese air pollution in two Canadian cities. *Environ. Res.,* **104,** 420–432.

Gaffin, S. R., and Coauthors, 2008: Variations in New York City's urban heat island strength over time and space. *Theor. Appl. Climatol.,* **94,** 1–11.

Gedzelman, S. D., S. Austin, R. Cermak, N. Stefano, S. Partridge, S. Quesenberry, and D. A. Robinson, 2003: Mesoscale aspects of the urban heat island around New York City. *Theor. Appl. Climatol.,* **75,** 29–42.

Gershunov, A., D. R. Cayan, and S. F. Iacobellis, 2009: The great 2006 heat wave over California and Nevada: Signal of an increasing trend. *J. Climate,* **22,** 6181–6203.

Golden, J. S., D. Hartz, A. Brazel, G. Luber, and P. Phelan, 2008: A biometeorology study of climate and heat-related morbidity in Phoenix from 2001 to 2006. *Int. J. Biometeor.,* **52,** 471–480.

Gosling, S., J. Lowe, G. McGregor, M. Pelling, and B. Malamud, 2009: Associations between elevated atmospheric temperature and human mortality: A critical review of the literature. *Climatic Change,* **92,** 299–341.

Grimmond, C. S. B., and T. R. Oke, 1995: Comparison of heat fluxes from summertime observations in the suburbs of four North American cities. *J. Appl. Meteor.,* **34,** 873–889.

——, and Coauthors, 2010: Climate and more sustainable cities: Climate information for improved planning and management of cities (producers/capabilities perspective). *Procedia Environ. Sci.,* **1,** 247–274.

Hajat, S., and T. Kosatky, 2010: Heat-related mortality: A review and exploration of heterogeneity. *J. Epidemiol. Community Health,* **64,** 735–760.

Hart, M. A., and D. J. Sailor, 2009: Quantifying the influence of land-use and surface characteristics on spatial variability in the urban heat island. *Theor. Appl. Climatol.,* **95,** 397–406.

Hobbs, F., and N. Stoops, 2002: Demographic trends in the 20th century. U.S. Census Bureau Census 2000 Special Reports, Series CENSR-4, 222 pp. [Available online at http://www.census.gov/prod/2002pubs/censr-4.pdf.]

Hoek, G., R. Beelen, K. de Hoogh, D. Vienneau, J. Gulliver, P. Fischer, and D. Briggs, 2008: A review of land-use regression models to assess spatial variation of outdoor air pollution. *Atmos. Environ.,* **42,** 7561–7578.

Huth, R., J. Kyselý, and L. Pokorná, 2000: A GCM simulation of heat waves, dry spells, and their relationships to circulation. *Climatic Change,* **46,** 29–60.

Jendritzky, G., A. Maarouf, and H. Staiger, 2001: Looking for a universal thermal climate index (UTCI) for outdoor applications. *Proc. Moving Thermal Comfort Standards into the 21st Century Conf.,* Windsor, United Kingdom, Oxford Centre for Sustainable Development, 353–367.

Kalkstein, L. S., and S. C. Sheridan, 2003: The impact of heat island reduction strategies on health-debilitating oppressive air masses in urban areas. U.S. EPA Heat Island Reduction Initiative Rep., 27 pp.

Karl, T. R., R. W. Knight, D. R. Easterling, and R. G. Quayle, 1996: Indices of climate change for the United States. *Bull. Amer. Meteor. Soc.,* **77,** 279–292.

Kim, Y. H., and J. J. Baik, 2005: Spatial and temporal structure of the urban heat island in Seoul. *J. Appl. Meteor.,* **44,** 591–605.

Kunkel, K. E., S. A. Changnon, B. C. Reinke, and R. W. Arritt, 1996: The July 1995 heat wave in the Midwest: A climatic perspective and critical weather factors. *Bull. Amer. Meteor. Soc.,* **77,** 1507–1518.

Kuttler, W., A. B. Barlag, and F. Robmann, 1996: Study of the thermal structure of a town in a narrow valley. *Atmos. Environ.,* **30,** 365–378.

MacDonald, C., 2011: Detroit targets services to healthy neighborhoods. *Detroit News,* 29 September, 1st ed., 1A. [Available online at http://www.detnews.com/article/20110929/METRO01/109290419.]

Magee, N., J. Curtis, and G. Wendler, 1999: The urban heat island effect at Fairbanks, Alaska. *Theor. Appl. Climatol.,* **64,** 39–47.

Mannarano, D., 1998: Automated Surface Observing System (ASOS) user's guide. National Oceanic and Atmospheric Administration, 72 pp. [Available online at http://www.nws.noaa.gov/asos/pdfs/aum-toc.pdf.]

Mohsin, T., and W. A. Gough, 2012: Characterization and estimation of urban heat island at Toronto: Impact of the choice of rural sites. *Theor. Appl. Climatol.,* **108,** 105–117.

Morris, C. J. G., I. Simmonds, and N. Plummer, 2001: Quantification of the influences of wind and cloud on the nocturnal urban heat island of a large city. *J. Appl. Meteor.,* **40,** 169–182.

National Climatic Data Center, cited 2010: NCDC GIS Map Services Index. [Available online at http://gis.ncdc.noaa.gov/maps/.]

National Weather Service, cited 2011: Southeast Michigan climatology. Detroit/Pontiac, Michigan, National Weather Service Weather Forecast Office. [Available online at http://www.crh.noaa.gov/dtx/climate.php.]

NWS Office of Climate, Weather, and Water Services, cited 2010a: Heat: A major killer. [Available online at http://www.nws.noaa.gov/om/heat/.]

——, cited 2010b: Natural Hazard Statistics. [Available online at http://www.weather.gov/os/hazstats.shtml.]

Observing Systems Branch, 1989: Cooperative station observations. National Weather Service Observing Handbook 2, 81 pp.

Oke, T. R., 1973: City size and the urban heat island. *Atmos. Environ.,* **7,** 769–779.

——, 1982: The energetic basis of the urban heat island. *Quart. J. Roy. Meteor. Soc.,* **108,** 1–24.

——, 2004: Initial guidance to obtain representative meteorological observations at urban sites. Instruments and Observing Methods Rep. 81, World Meteorological Organization Tech. Doc. WMO/TD-1250, 51 pp. [Available online at http://www.wmo.int/pages/prog/www/IMOP/publications/IOM-81/IOM-81-UrbanMetObs.pdf.]

Peterson, T. C., 2003: Assessment of urban versus rural in situ surface temperatures in the contiguous United States: No difference found. *J. Climate,* **16,** 2941–2959.

——, and T. W. Owen, 2005: Urban heat island assessment: Metadata are important. *J. Climate,* **18,** 2637–2646.

Runnalls, K. E., and T. R. Oke, 2000: Dynamics and controls of the near-surface heat island of Vancouver, British Columbia. *Phys. Geogr.,* **21,** 283–304.

Ryan, B. D., 2008: The restructuring of Detroit: City block form change in a shrinking city, 1900-2000. *Urban Des. Int.,* **13,** 156–168.

Saaroni, H., E. Ben-Dor, A. Bitan, and O. Potchter, 2000: Spatial distribution and microscale characteristics of the urban heat island in Tel-Aviv, Israel. *Landscape Urban Plann.,* **48,** 1–18.

Sanderson, M., I. Kumanan, T. Tanguay, and W. Schertzer, 1973: Three aspects of the urban climate of Detroit-Windsor. *J. Appl. Meteor.,* **12,** 629–638.

Sheridan, S. C., 2002: The redevelopment of a weather-type classification scheme for North America. *Int. J. Climatol.,* **22,** 51–68.

——, cited 2010: Spatial synoptic classification. [Available online at http://sheridan.geog.kent.edu/ssc.html.]

Spearman, C. E., 1907: Demonstration of formulae for true measurement of correlation. *Amer. J. Psychol.,* **18,** 161–169.

Steadman, R. G., 1984: A universal scale of apparent temperature. *J. Climate Appl. Meteor.,* **23,** 1674–1687.

Stone, B., J. J. Hess, and H. Frumkin, 2010: Urban form and extreme heat events: Are sprawling cities more vulnerable to climate change than compact cities? *Environ. Health Perspect.,* **118,** 1425–1428.

United Nations Population Division, cited 2010: World urbanization prospects: The 2007 revision population database. [Available online at http://esa.un.org/unup/.]

U.S. Geological Survey, cited 2008: National Land Cover Database: Multi-Resolution Land Characteristics Consortium (MRLC). [Available online at http://gisdata.usgs.gov/website/mrlc/viewer.htm?.]

Whiteman, C. D., J. M. Hubbe, and W. J. Shaw, 2000: Evaluation of an inexpensive temperature datalogger for meteorological applications. *J. Atmos. Oceanic Technol.,* **17,** 77–81.

Wilby, R. L., 2003: Past and projected trends in London's urban heat island. *Weather,* **58,** 251–260.

Wilhelmi, O. V., K. L. Purvis, and R. C. Harriss, 2004: Designing a geospatial information infrastructure for mitigation of heat wave hazards in urban areas. *Nat. Hazards Rev.,* **5,** 147–158.

Wong, N. H., and C. Yu, 2005: Study of green areas and urban heat island in a tropical city. *Habitat Int.,* **29,** 547–558.

Yagüe, C., E. Zurita, and A. Martinez, 1991: Statistical analysis of the Madrid urban heat island. *Atmos. Environ.,* **25B,** 327–332.

Yokobori, T., and S. Ohta, 2009: Effect of land cover on air temperatures involved in the development of an intra-urban heat island. *Climate Res.,* **39,** 61–73.

Zhang, K., E. Oswald, D. Brown, S. Brines, C. Gronlund, J. White-Newsome, R. Rood, and M. O'Neill, 2011: Geostatistical exploration of spatial variation of summertime temperatures in the Detroit metropolitan region. *Environ. Res.,* **111,** 1046–1053.